Elemental Fractionation in Ultraviolet Laser Ablation of Igneous Silicate Minerals Relevant to Mars

M.E. Taylor, D.L. Blaney, and G. Cardell

Jet Propulsion Laboratory, Pasadena, CA 91109

Abstract – Laser ablation has significant potential for terrestrial and extraterrestrial remote sampling applications if elemental fractionation can be understood and controlled. This study focuses on acmite, albite, augite, diopside, forsterite, and labradorite, igneous silicate minerals that are relevant to Mars, Earth, the moon, and asteroids. The minerals were ablated using a frequency-quadrupled Nd:YAG laser (266 nm) and the ablation products were captured on graphite substrates as films. Rutherford backscattering spectrometry (RBS) and electron spectroscopy for chemical analysis (ESCA) measurements of the minerals and their films indicate that the fractionation effects are small. The largest fractionation effects occur for Na, Ca, and Fe and are qualitatively consistent with a mineral surface conditioning mechanism. Films of albite and labradorite, plagioclase feldspars with similar nominal compositions, are easily distinguished. Films of acmite, augite, and diopside, clinopyroxenes with similar nominal compositions, are also easily distinguished.

2

INTRODUCTION

Laser ablation is a technique that is often used to obtain vapor-phase material for subsequent chemical analysis (Miller and Haglund, 1998; Chrisey and Hubler, 1994; Vertes et al., 1993; Moenke-Blankenburg, 1989). Chemical information is obtained through either direct or indirect analysis of the ablation products. Direct approaches include optical spectroscopy and time-of-flight mass spectrometry (Kelly et al., 1998; Geohegan, 1994). In some indirect approaches, i.e. inductively coupled plasma atomic emission spectrometry (ICP-AES) and inductively coupled plasma mass spectrometry (ICP-MS), the ablation products are introduced into an additional excitation source (Russo and Mao, 1998; Jarvis and Jarvis, 1992). In other indirect approaches the ablation products are captured on a substrate, a process called pulsed laser deposition (PLD) (Miller and Haglund, 1998; Chrisey and Hubler, 1994). The resulting films are analyzed by standard characterization techniques, i.e. Rutherford backscattering spectrometry (RBS) and electron spectroscopy for chemical analysis (ESCA), also called x-ray photoelectron spectroscopy (XPS) (Schleberger et al., 1998; Feldman and Mayer, 1986; Chu et al., 1978).

Laser ablation is particularly feasible for chemical analysis of geological materials. It can be used to sample both conducting and insulating materials and is therefore applicable to a wide variety of rocks and minerals. Since extensive material preparation is not required, measurement time and opportunities for accidental contamination are minimal. Ablation crater diameters of a few tens of micrometers and ablation rates of a few nanometers per pulse are not unusual, making both spatial profiling and depth profiling possible.

Elemental fractionation in laser ablation has been studied for a variety of geological materials (Jeffries et al., 1996; Jarvis and Williams, 1993; Moenke-Blankenburg and Günther, 1992). The majority of these studies used ICP-AES and ICP-MS techniques and focused on trace element fractionation. Photon absorption efficiency was found to vary from mineral to mineral, more significantly for infrared ablation and less significantly for ultraviolet ablation. Fractionation effects were found to correlate with absorbed power density and are more significant for infrared ablation than for ultraviolet ablation.

Elemental fractionation traditionally attributed to laser ablation may arise in part from other sources. In ICP-AES and ICP-MS, for example, fractionation may occur during transport to the ICP or in the ICP. Recent ICP-MS measurements suggest that large particulates are often either lost during transport to the ICP or incompletely digested in the ICP and that this can result in fractionation (Alexander et al., 1998; Figg et al., 1998; Goodall et al., 1995).

Laser ablation has significant potential for terrestrial and extraterrestrial remote sampling applications if elemental fractionation can be understood and controlled. This study was undertaken with that objective. A PLD approach rather than an ICP-AES or ICP-MS approach was selected to avoid potential fractionation related to the ICP.

MINERAL SELECTION AND PREPARATION

The Shergottite-Nakhlite-Chassignite (SNC) meteorites are believed to have originated on Mars and are reported to consist largely of feldspars, pyroxenes, and olivines (McSween, 1994). The Earth's continental crust is reported to consist of 58%

feldspars, 13% pyroxenes and amphiboles, and 3% olivines by volume (Ernst, 1969). These types of minerals are also relevant to the moon and asteroids. They are therefore of general interest for terrestrial and extraterrestrial remote sampling applications.

Acmite, albite, augite, diopside, forsterite, and labradorite were selected for this study. Albite and labradorite are plagioclase feldspars, acmite, augite, and diopside are clinopyroxenes, and forsterite is an olivine. The nominal compositions of these minerals are shown in Tab 1 (Chesterman, 1995).

All specimens used in this study are research grade natural specimens. Multiple specimens of each mineral were polished using silicon carbide films with average particulate diameters of 68 μm, 22 μm, and 14 μm and diamond films with average particulate diameters of 6 μm, 3 μm, and 1 μm.

EXPERIMENTS

The experimental setup is shown in Fig 1. The ablation laser is a pulsed frequency-quadrupled Nd:YAG laser with an internal energy attenuator. The wavelength, pulse repetition rate, maximum pulse energy, and temporal pulse width are specified as 266 nm, 15 Hz, 5 mJ, and 3-5 ns, respectively, and the pulse spatial and temporal profiles are specified as Gaussian. The mineral target and the graphite substrate are separated by approximately 2.5 cm and are housed in a vacuum chamber with a typical pressure of 5×10^{-8} Torr. The laser is focused to approximately 0.4 mm^2 at the target surface. Prior to ablation, the average powers incident on the target and reflected from the target are measured using a thermopile meter. During ablation, the position of the target is adjusted

at intervals of 4500 pulses to provide a fresh target area. Ablation is stopped when a film is visible on the substrate.

Films were deposited from acmite, albite, augite, diopside, and forsterite targets at nominal power densities of 100 MWcm^{-2} and 320 MWcm^{-2} and from a labradorite target at a nominal power density of 320 MWcm^{-2}. A nominal power density of 100 MWcm^{-2} was insufficient to achieve a visible ablation plume in the case of labradorite. For each experiment Tab 2 shows the power density calculated from the thermopile measurements for a temporal pulse width of 4 ns and an area of 0.4 mm^2. This power density varies primarily because of variations in target reflectivity arising from composition and surface roughness.

CHARACTERIZATION

In RBS the sample is irradiated with monochromatic ions (Schleberger et al., 1998; Feldman and Mayer, 1986; Chu et al., 1978). The ions undergo Coulomb repulsion collisions with the sample atoms and are backscattered. The energy loss of each backscattered ion is a function of the energy lost prior to the backscattering collision, determined by the penetration depth and the mass and density of the sample atoms, and the energy lost in the backscattering collision, determined by the mass of the sample atom with which it collides, and is relatively independent of the chemical environments of the sample atoms. The effective sampling depth is typically a micrometer. The RBS system used in this study produces a beam of 2 MeV He^{+2} ions with a sampling area of approximately 25 mm^2.

In ESCA the sample is irradiated with monochromatic x-rays (Schleberger et al., 1998; Feldman and Mayer, 1986). The sample atom electrons absorb the x-rays and are ejected. The energy of each ejected electron is determined by the electron binding energy and is therefore a function of the sample atoms and their chemical environments. The effective sampling depth is limited by the escape depth of the ejected electrons and is typically several nanometers. Because ESCA has a small effective sampling depth surface contamination may affect results. Samples are often exposed to an ion beam just prior to characterization to sputter-clean their surfaces. The ESCA system used in this study produces a focused beam of 1486.6 eV Al $K\alpha$ x-rays with a sampling area of approximately 0.3 mm^2 for characterization and a beam of Ar$^+$ ions for removal of surface contamination.

RBS was selected as the primary characterization technique for this study because large sampling depth, large sampling area, and insensitivity to chemical environment make RBS preferable to ESCA for mean composition measurements. All targets and films were characterized by RBS and selected targets and films were characterized by ESCA. Ablated targets were polished prior to characterization to eliminate material potentially affected by the ablation process. To evaluate the variations in composition between and within targets, two targets of each mineral were characterized by RBS and one target of each mineral was characterized by RBS, polished, and characterized again by RBS. To remove surface contamination 5 nm of material was sputtered from the surfaces of targets and films characterized by ESCA. This was found to less effective for the targets than for the films, possibly because of shadowing effects arising from greater

surface roughness. For the targets, five areas within the sputtered area were characterized to compensate for variations in composition arising from surface contamination.

RESULTS

To demonstrate the ability of RBS to accurately indicate composition, a specimen of NIST 1830 was polished and characterized. Tab 3 shows the composition indicated by NIST and the composition obtained from a fit to the RBS spectrum. The uncertainty shown for the latter composition is the two-sigma uncertainty in the fit. For each element, the value indicated by RBS differs from the value indicated by NIST by less than the uncertainty in the RBS value.

The compositions indicated by RBS and ESCA for the targets and films are shown in Tabs 4(a) and 4(b) and in Figs 2(a), 2(b), and 2(c). Each film composition was obtained from a fit to a RBS or ESCA spectrum and the uncertainty shown is the two-sigma uncertainty in the fit. RBS indicated that for all of the minerals variations in composition between targets were not significant in comparison to variations in composition within a target. For RBS each target composition is the mean of three compositions obtained from fits to spectra collected from multiple targets. For ESCA each target composition is the mean of five compositions obtained from fits to spectra collected from multiple areas on a target. The uncertainty shown for each of the target compositions is the two-sigma uncertainty in the mean.

Neither RBS nor ESCA provides complete composition information for all of the minerals and their failures should be noted. RBS is unable to distinguish the small Al signals from the large Si signals in the albite and labradorite films and is therefore unable

to provide stable Al values for those films. In ESCA the O signals are unstable for the targets, possibly due to surface contamination or preferential sputtering, and ESCA is therefore unable to provide O values for the targets. In RBS the compositions for the albite and labradorite films are normalized to the Al values for the corresponding targets. In ESCA the compositions for the targets are normalized to the O values for the corresponding films.

The compositions indicated by RBS and ESCA differ slightly. These deviations are not atypical and most likely occur because elemental sensitivity varies with factors such as chemical environment. In this study the relative compositions of the targets and films are of interest and therefore differences in the compositions indicated by the two techniques are not of moment.

Albite and labradorite are plagioclase feldspars and are similar in composition. RBS indicates that the albite films are depleted in Ca and enriched in Na. ESCA confirms these effects in the film deposited at the higher power density. The labradorite film may also be enriched in Na but this effect is smaller than the uncertainty. Acmite, augite, and diopside are clinopyroxenes. For acmite RBS indicates that the films are depleted in Na, the film deposited at the lower power density is enriched in Si and Fe, and the film deposited at the higher power density is enriched in Ca. The films deposited at the lower and higher power densities may also be enriched in Ca and Si, respectively, but these effects are smaller than the uncertainties. ESCA confirms the Na and Ca effects in the film deposited at the higher power density. For augite RBS indicates that the films are depleted in Fe and the film deposited at the higher power density is enriched in Si and Ca. The film deposited at the lower power density may also be enriched in Si and Ca but this

effect is smaller than the uncertainty. ESCA confirms the Ca and Fe effects in the film deposited at the higher power density. For diopside RBS indicates that the films are enriched in Ca and the film deposited at the lower power density is depleted in Mg. The films may also be depleted in Fe and the film deposited at the higher power density may also be depleted in Mg but these effects are smaller than the uncertainties. Forsterite is an olivine. RBS indicates that the films are depleted in Mg. To check for additional effects masked by these effects, the film values for the relevant elements were set equal to the corresponding target values and the RBS compositions were renormalized. No additional effects became apparent.

DISCUSSION

Each of the minerals included in this study is comprised of a structural framework of tetrahedrons. Each tetrahedron is comprised of a central Si atom bonded to four O atoms. In olivines the tetrahedrons are isolated and the structural unit is SiO_4^{-4}. In clinopyroxenes two Si^{+4} share every other O^{-2} and the structural unit is SiO_3^{-2}. In plagioclase feldspars two Si^{+4} share every O^{-2} and the structural unit is SiO_2. However, Si^{+4} is replaced by Al^{+3} in one quarter to one half of the tetrahedrons to produce AlO_2^{-1}.

The O atoms in the structural units bond to cations to compensate for charge imbalance. In olivines the cations, typically Mg^{+2} and Fe^{+2}, are located in small sites with six-fold coordination. In clinopyroxenes there are two types of cation sites, small sites with six-fold coordination and large sites with eight-fold coordination. Mg^{+2}, Fe^{+2}, and Fe^{+3} typically occupy the first type of site; Na^+ and Ca^{+2} typically occupy the second type

of site. In plagioclase feldspars the cations, typically Na^+ and Ca^{+2}, are located in large sites with six-fold or seven-fold coordination.

The array of silicate mineral compositions produced in nature occurs because the cations Na^+, Mg^{+2}, Ca^{+2}, Fe^{+2}, and Fe^{+3} are exchangeable within physical and electronic limits (Ernst, 1969). Cations are physically exchangeable if they have similar ionic radii. Ionic radii for these cations are shown in Tab 5. Na^+ and Ca^{+2} have similar radii and Mg^{+2} and Fe^{+3} have similar radii. Fe^{+2} has an intermediate radius slightly larger than that of Mg^{+2} and Fe^{+3}. Cations are electronically exchangeable if they have identical charge states. A pair of cations in spatially proximate sites may be electronically exchangeable with another pair of cations if both pairs have identical total charge states.

Fractionation effects observed in previous studies have been attributed to thermal and photochemical conditioning of the target surface (Jeffries et al., 1996; Ball and Sauerbrey, 1998; Russo and Mao, 1998; Mao et al., 1998). The ablation rate, estimated from measurements of film volume and adjusted to compensate for loss of material between the target and the substrate, is on the order of 1 nm per pulse. A large fraction of material that is eventually ablated is surface material prior to ablation, and is therefore exposed to an incident power density that varies with position and time. A target surface conditioning mechanism based on preferential desorption of cations followed by preferential adsorption of cations from a reservoir of previously desorbed or ablated cations may be responsible for the fractionation effects observed in this study. For each type of cation site there is a set of primary cations and a set of secondary cations. Members of both sets can occupy the sites but members of the primary set are energetically preferred. Primary cations may be less likely to be desorbed and more likely

to be adsorbed than secondary cations. Since desorbed atoms lack the energy and directionality of ablated atoms and are less likely to be collected on the substrate, the film composition should reflect the conditioned target composition.

To identify the largest fractionation effects the ratios R_1 and R_2

$$R_1 = (F - T) / T$$

$$R_2 = |F - T| / (f + t)$$

were calculated for the effects noted previously. RBS values were used. F is the film value, T is the target value, f is the uncertainty in the film value, and t is the uncertainty in the target value. R_1 and R_2 are shown in Fig 3. Data above and below the origin correspond to enrichment and depletion effects, respectively. The largest effects correspond to Na, Ca, and Fe and occur in augite, diopside, acmite, and albite.

These effects are qualitatively consistent with the proposed target surface conditioning mechanism. The RBS data for the augite and diopside targets suggests that some of the large cation sites are occupied by Fe^{+2} rather than by Ca^{+2}. Fe^{+2} may be a secondary cation rather than a primary cation because of smaller ionic radius. As a result Fe^{+2} may be preferentially desorbed and Ca^{+2} may be preferentially adsorbed, leading to Fe depletion and Ca enrichment at the target surface and in the films. The RBS data for the acmite targets suggests that some of the pairs of large and small cation sites are occupied by Na^+ and Fe^{+3} pairs rather than by Ca^{+2} and Fe^{+2} pairs. Na^+ and Fe^{+3} may be a secondary cation pair rather than a primary cation pair because of charge separation. As a result Na^+ may be preferentially desorbed, Ca^{+2} may be preferentially adsorbed, and Fe^{+3} may be converted to Fe^{+2} to compensate for charge imbalance, leading to Na depletion and Ca enrichment at the target surface and in the films. In the albite targets, to

compensate for charge imbalance, Na^+ bonds to AlO_2^{-1} or Ca^{+2} bonds to pairs of AlO_2^{-1}. Ca^{+2} may be a secondary cation rather than a primary cation because it must bond to a pair of AlO_2^{-1} rather than to a single AlO_2^{-1}. As a result Ca^{+2} may be preferentially desorbed and Na^+ may be preferentially adsorbed, leading to Ca depletion and Na enrichment at the target surface and in the films. The Na effect is larger than the Ca effect because a pair of Na^+ are adsorbed for every Ca^{+2} that is desorbed.

CONCLUSIONS

The fractionation effects observed in this study are small. The largest fractionation effects occur for Na, Ca, and Fe and are qualitatively consistent with a target surface conditioning mechanism. Films of albite and labradorite, which have similar nominal compositions, are easily distinguished. Films of acmite, augite, and diopside, which have similar nominal compositions, are also easily distinguished.

These results are of interest because they indicate that ultraviolet laser ablation is a feasible technique for sampling feldspars, pyroxenes, and olivines. These types of minerals are major constituents of Mars, Earth, the moon, and asteroids. Therefore these results indicate that ultraviolet laser ablation is a feasible technique for a variety of terrestrial and extraterrestrial remote sampling applications.

REFERENCES

Alexander M. L., Smith M. R., Hartman J. S., Mendoza A., and Koppenaal D. W. (1998) Laser ablation inductively coupled plasma mass spectrometry. *Appl. Surf. Sci.* **127-129**, 255-261.

Ball Z. and Sauerbrey R. (1998) Surface modification with lasers. In *Laser Ablation and Desorption* (ed. J. C. Miller et al.). Vol. 30. Chap. 7, pp. 333-373. Academic Press.

Chesterman C. W. (1995) *National Audubon Society Field Guide to North American Rocks and Minerals*. Chanticleer Press.

Chrisey D. B. and Hubler G. K. (1994) *Pulsed Laser Deposition of Thin Films*. John Wiley and Sons.

Chu W. K., Mayer J. W., and Nicolet M. A. (1978) *Backscattering Spectrometry*. Academic Press.

Ernst W. G. (1969) *Earth Materials*. Prentice Hall.

Feldman L. C. and Mayer J. W. (1986) *Fundamentals of Surface and Thin Film Analysis*. Prentice Hall.

Figg D. J., Cross J. B., and Brink C. (1998) More investigations into elemental fractionation resulting from laser ablation inductively coupled plasma mass spectrometry on glass samples. *Appl. Surf. Sci.* **127-129**, 287-291.

Geohegan D. B. (1994) Diagnostics and characteristics of laser-produced plasmas. In *Pulsed Laser Deposition of Thin Films* (ed. D. B. Chrisey et al.). Chap. 5, pp. 115-165. John Wiley and Sons.

Goodall P., Johnson S. G., and Wood E. (1995) Laser ablation inductively coupled plasma atomic emission spectrometry of an uranium-zirconium alloy: Ablation properties and analytical behavior. *Spectrochim. Acta* **50B**, 1823-1835.

Jarvis I. and Jarvis K. E. (1992) Plasma spectrometry in the earth sciences: Techniques, applications and future trends. *Chem. Geol.* **95**, 1-33.

Jarvis K. E. and Williams J. G. (1993) Laser ablation inductively coupled plasma mass spectrometry (LA-ICP-MS): A rapid technique for the direct, quantitative determination of major, trace and rare-earth elements in geological samples. *Chem. Geol.* **106**, 251-262.

Jeffries T. E., Pearce N. J. G., Perkins W. T., and Raith A. (1996) Chemical fractionation during infrared and ultraviolet laser ablation inductively coupled plasma mass spectrometry – Implications for mineral microanalysis. *Anal. Comm.* **33**, 35-39.

Kelly R., Miotello A., Mele A., and Giardini Guidoni A. (1998) Plume formation and characterization in laser-surface interactions. In *Laser Ablation and Desorption* (ed. J. C. Miller et al.). Vol. 30. Chap. 5, pp. 225-289. Academic Press.

Mao X. L., Ciocan A. C., and Russo R. E. (1998) Preferential vaporization during laser ablation inductively coupled plasma atomic emission spectroscopy, *Appl. Spectrosc.* **52**, 913-918.

McSween H. Y., Jr. (1994) What we have learned about Mars from SNC meteorites. *Meteoritics* **29**, 757-779.

Miller J. C. and Haglund R. F. (1998) *Laser Ablation and Desorption*. Vol. 30. Academic Press.

Moenke-Blankenburg L. (1989) *Laser Microanalysis*. Vol. 105. John Wiley and Sons.

Moenke-Blankenburg L. and Günther D. (1992) Laser microanalysis of geological samples by atomic emission spectrometry (LM-AES) and inductively coupled plasma – atomic emission spectrometry (LM-ICP-AES). *Chem. Geol.* **95**, 85-92.

Russo R. E. and Mao X. L. (1998) Chemical analysis by laser ablation. In *Laser Ablation and Desorption* (ed. J. C. Miller et al.). Vol. 30. Chap. 8, pp. 375-412. Academic Press.

Schleberger M., Speller S., and Heiland W. (1998) Surface characterization. In *Laser Ablation and Desorption* (ed. J. C. Miller et al.). Vol. 30. Chap. 6, pp. 291-331. Academic Press.

Vertes A., Gijbels R., and Adams F. (1993) *Laser Ionization Mass Analysis*. Vol. 124. John Wiley and Sons.

Table 1: Silicate minerals selected for this study (Chesterman, 1995).

Mineral	Classification	Nominal Composition
Acmite	Clinopyroxene	$NaFeSi_2O_6$
Albite	Plagioclase Feldspar	$NaAlSi_3O_8$
Augite	Clinopyroxene	$(Ca,Na)(Mg,Fe)Si_2O_6$
Diopside	Clinopyroxene	$CaMgSi_2O_6$
Forsterite	Olivine	Mg_2SiO_4
Labradorite	Plagioclase Feldspar	30% $NaAlSi_3O_8$ 70% $CaAl_2Si_2O_8$

Table 2: Ablation power densities used in this study.

Silicate Mineral	Nominal Value 100 MWcm^{-2}	Nominal Value 320 MWcm^{-2}
Acmite	71 MWcm^{-2}	269 MWcm^{-2}
Albite	90 MWcm^{-2}	314 MWcm^{-2}
Augite	77 MWcm^{-2}	282 MWcm^{-2}
Diopside	77 MWcm^{-2}	282 MWcm^{-2}
Forsterite	90 MWcm^{-2}	314 MWcm^{-2}
Labradorite		276 MWcm^{-2}

Table 3: NIST 1830 compositions in atomic percents as indicated by NIST and RBS.

Element	NIST	RBS
O	60.5	60.7 ± 1.7
Na	9.2	9.2 ± 0.7
Mg	2.0	1.8 ± 0.6
Si	25.2	25.0 ± 0.6
Ca	3.2	3.3 ± 0.1

Table 4(a): Compositions in atomic percents as indicated by RBS for silicate mineral targets (upper) and films deposited at nominal power densities of 100 MWcm^{-2} (center) and 320 MWcm^{-2} (lower).

Element	Acmite	Albite	Augite	Diopside	Forsterite	Labradorite
O	59.1 ± 1.5	62.1 ± 0.2	59.6 ± 1.0	59.9 ± 0.3	57.2 ± 0.8	61.9 ± 0.8
	58.2 ± 1.4	62.0 ± 2.8	60.2 ± 2.3	60.4 ± 2.3	57.4 ± 1.6	
	59.1 ± 0.9	60.9 ± 1.7	57.6 ± 1.0	58.2 ± 1.4	57.3 ± 1.6	61.2 ± 1.9
Na	4.7 ± 1.0	7.7 ± 0.3				2.7 ± 1.1
	2.6 ± 0.3	9.2 ± 0.6				
	2.7 ± 0.2	9.4 ± 0.5				3.5 ± 0.3
Mg	4.6 ± 1.3		7.6 ± 0.2	10.0 ± 0.4	25.7 ± 0.1	
	4.6 ± 0.3		7.6 ± 0.5	8.9 ± 0.5	24.3 ± 0.8	
	4.4 ± 0.3		7.6 ± 0.2	9.6 ± 0.4	24.5 ± 0.8	
Al		6.3 ± 1.2				12.0 ± 1.3
		6.3				
		6.3				12.0
Si	19.3 ± 1.5	23.5 ± 0.9	19.2 ± 0.3	19.9 ± 0.3	13.9 ± 0.8	18.4 ± 1.2
	21.4 ± 0.5	22.4 ± 1.0	19.5 ± 0.7	19.1 ± 0.7	15.0 ± 0.5	
	20.5 ± 0.3	23.3 ± 0.8	20.3 ± 0.3	19.6 ± 0.5	14.8 ± 0.5	18.4 ± 0.7
Ca	6.6 ± 0.7	0.4 ± 0.0	9.1 ± 0.8	9.1 ± 0.2		4.8 ± 0.2
	7.0 ± 0.2	0.1 ± 0.1	9.4 ± 0.3	10.8 ± 0.4		
	7.8 ± 0.2	0.1 ± 0.1	10.8 ± 0.2	11.8 ± 0.3		4.8 ± 0.1
Fe	5.7 ± 0.3		4.5 ± 0.3	1.1 ± 0.2	3.2 ± 0.1	0.2 ± 0.0
	6.2 ± 0.1		3.3 ± 0.1	0.8 ± 0.1	3.3 ± 0.1	
	5.5 ± 0.1		3.7 ± 0.1	0.8 ± 0.1	3.4 ± 0.1	0.1 ± 0.1

Table 4(b): Compositions in atomic percents as indicated by ESCA for silicate mineral targets (upper) and films deposited at a nominal power densities of 320 MWcm^{-2} (lower).

Element	Acmite	Albite	Augite
O	61.31	61.53	62.16
	61.31 ± 0.35	61.53 ± 0.31	62.16 ± 0.32
Na	2.39 ± 0.68	3.52 ± 0.41	
	1.58 ± 0.04	8.88 ± 0.09	
Mg	3.48 ± 0.96		5.13 ± 0.32
	3.93 ± 0.15		5.62 ± 0.16
Al		8.05 ± 0.25	
		8.26 ± 0.19	
Si	20.42 ± 0.68	25.89 ± 0.82	21.17 ± 0.49
	20.41 ± 0.27	21.20 ± 0.25	19.45 ± 0.24
Ca	7.03 ± 1.67	1.01 ± 0.09	7.69 ± 0.81
	8.72 ± 0.15	0.13 ± 0.02	10.24 ± 0.15
Fe	5.37 ± 0.32		3.85 ± 0.26
	4.05 ± 0.05		2.53 ± 0.04

Table 5: Common ions (Ernst, 1969).

Ion	Radius (Å)	Coordination
Na^+	0.97	6
Na^+	1.01	8
Mg^{+2}	0.66	6
Ca^{+2}	0.99	6
Ca^{+2}	1.03	8
Fe^{+2}	0.74	6
Fe^{+3}	0.64	6

FIGURE CAPTIONS

Figure 1: Experimental setup.

Figure 2: Compositions in atomic percents for silicate mineral targets and films deposited at nominal power densities of (a) 100 $MWcm^{-2}$ and (b) 320 $MWcm^{-2}$ as indicated by RBS, and for silicate mineral targets and films deposited at a nominal power density of (c) 320 $MWcm^{-2}$ as indicated by ESCA. The values are displaced along the horizontal axis for display. Where no fractionation is observed the values lie on the indicator lines.

Figure 3: R_1 and R_2 are functions that describe fractionation effects. R_1 is the ratio of the difference between the film and target values to the target value. R_2 is the ratio of the absolute value of the difference between the film and target values to the sum of the uncertainties in the film and target values. The values indicated by RBS, shown in Tab 4(a), are used to calculate R_1 and R_2. Data above and below the origin correspond to enrichment and depletion effects, respectively.
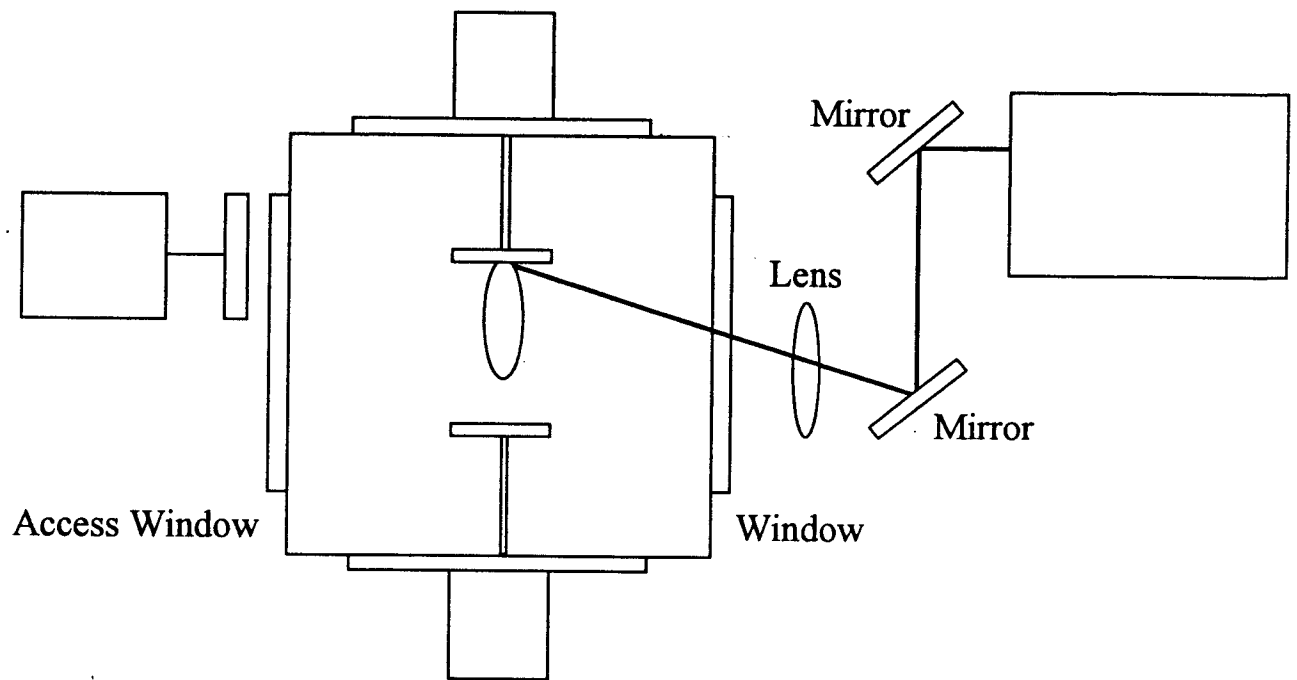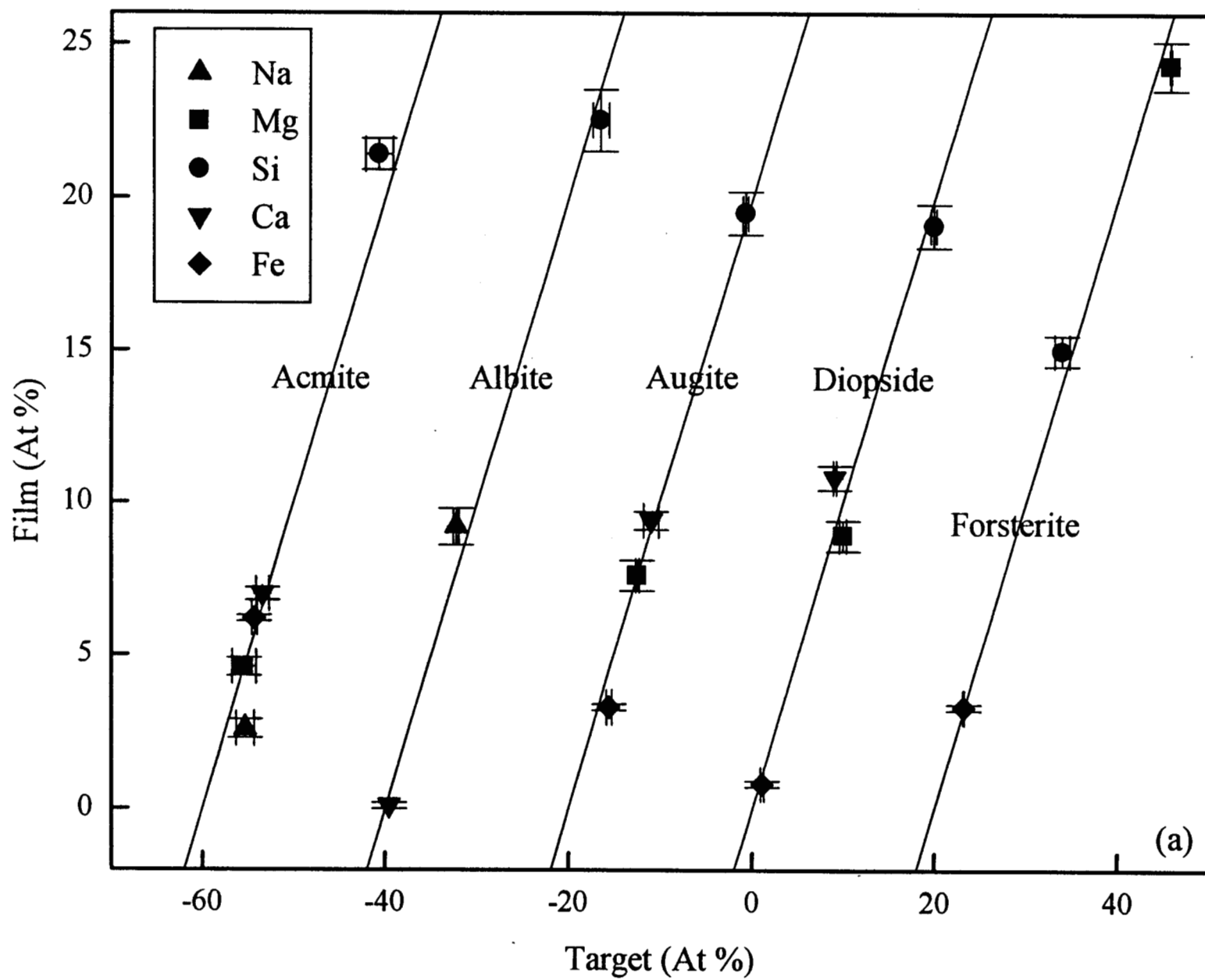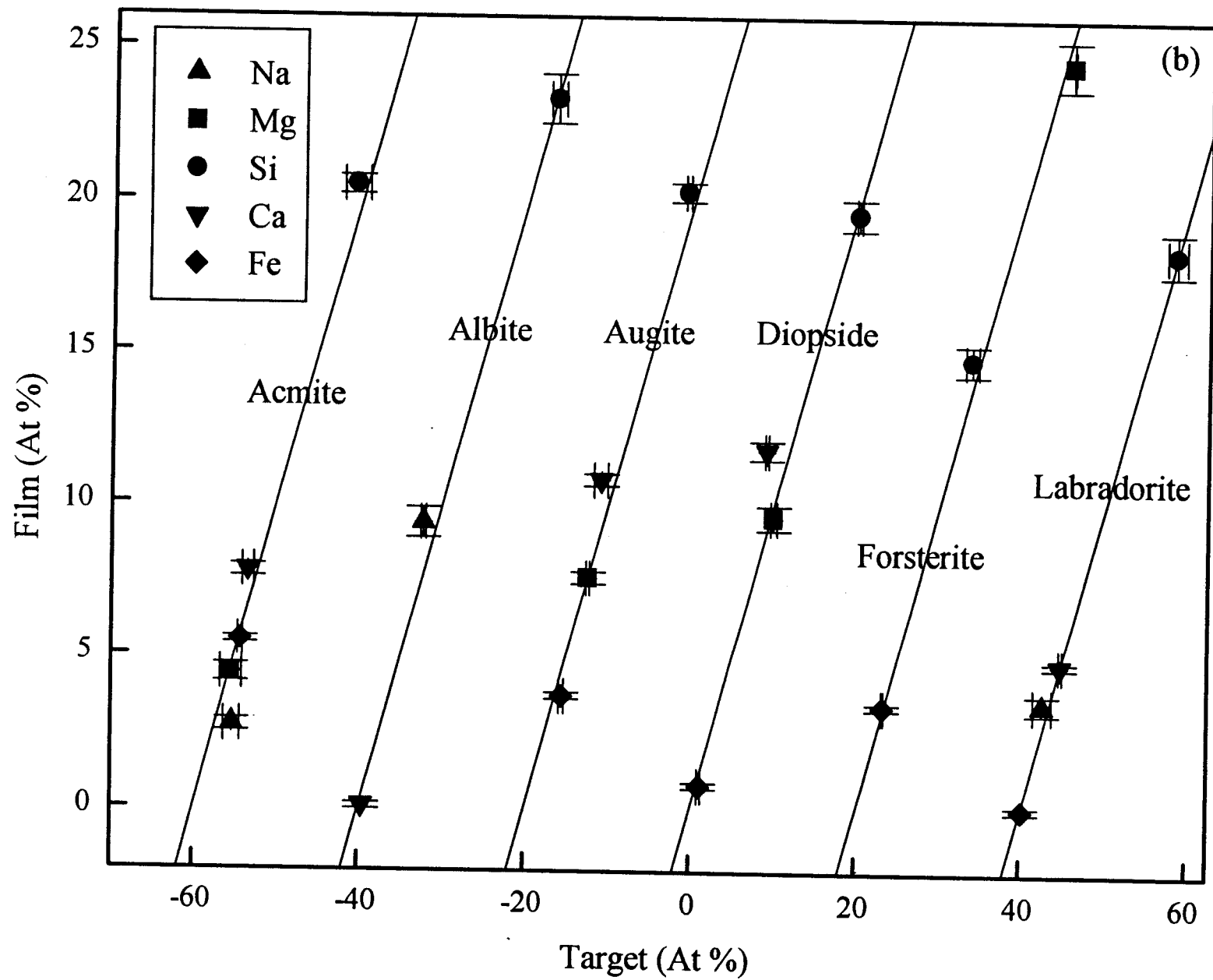
Fig 1

Mirror

Lens

Mirror

Access Window

Window

(a)

Fig 2(b)

(b)

Fig 2(c)

Fig 3